Desalination and Water Treatment
www.deswater.com
doi: 10.5004/dwt.2021.27641

240 (2021) 75–88
November

Fluoride removal by nanofiltration: experimentation, modelling and prediction based on the surface response method

Fatima Zahra Addar[a], Soufiane El-Ghzizel[a], Mustapha Tahaikt[a], Mustapha Belfaquir[a], Mohamed Taky[a,b,*], Azzedine Elmidaoui[a]

[a]*Laboratory of Advanced Materials and Process Engineering, Faculty of Sciences, Ibn Tofail University, P.O. Box: 1246, Kenitra, Morocco, emails: mohamed.taky@uit.ac.ma (M. Taky), Fatimazahra.addar@uit.ac.ma (F.Z. Addar), soufian.el-ghzizel@uit.ac.ma (S. El-Ghzizel), mustapha.tahaikt@uit.ac.ma (M. Tahaikt), Mustapha.belfaquir@uit.ac.ma (M. Belfaquir), elmidaoui@uit.ac.ma (A. Elmidaoui)*
[b]*International Water Research Institute, Mohammed VI Polytechnic University, Lot 660, Hay Moulay Rachid, Ben Guerir, 43150 – Morocco*

Received 11 May 2021; Accepted 25 July 2021

ABSTRACT

Fluoride ions contamination of groundwater becomes more and more a worldwide preoccupation, especially in Morocco. Indeed, they constitute a potential risk that can have adverse effects on human health (for instance, dental fluorosis, skeletal fluorosis, osteosarcoma, etc.) and effects on water resources. The aims of this study are to compare and evaluate the performance of three membranes in the removal of fluorides by nanofiltration (NF) on NaF doped groundwater. In the first part of this study, the influence of different operating conditions (initial fluoride concentration and transmembrane pressure) on the reduction of fluoride ions is investigated. Secondly, three separate predictive models are developed for optimization and modeling of the permeate concentration (mg L^{-1}), fluoride rejection (%) and permeate flux (L m^{-2} h^{-1}) in NF. Response surface methodology based on central composite design is employed to experimental design and a cumulative study of the effects of various operating parameters such as initial fluoride concentration and transmembrane pressure. Analysis of variance for developed quadratic models exhibits high significance and applicability. The initial fluoride concentration is the most significant factor that has a predominant effect on the permeate concentration for both TR60 and NF270 membranes. Indeed, both membranes exceed the standards, 7 mg L^{-1} for TR60 and 5.5 mg L^{-1} for NF270. But for NF90 the influence of the initial fluoride concentration is not significant. In addition, the model is analysed graphically for its predictive ability. Finally, under optimized conditions, fluoride rejection obtained are 79.69%, 72% and 98.75% for TR60, NF270 and NF90 respectively.

Keywords: Nanofiltration; Fluoride removal; Response surface methodology; Central composite design; Optimization

1. Introduction

Water is required for all living things in the world. There is a lot of water on the surface of the Earth, but the chemical composition of water is one of the important factors that make it unsafe for consumption [1]. Recent reports from UNICEF and WHO have confirmed that an estimated 748 million people do not have access to safe drinking water, while more than 1.8 billion people use water contaminated with fecal matter for drinking purposes [2]. Freshwater comes from groundwater and surface water, groundwater representing only 0.6% of total water resources,

* Corresponding author.

Presented at the Second International Symposium on Nanomaterials and Membrane Science for Water, Energy and Environment (SNMS-2021), June 1–2, 2022, Tangier, Morocco

which are polluted due to intense industrialization, population growth and urbanization activities [3]. Numerous contaminations are present in groundwater, such as fluoride, arsenic, iron, lead, cadmium, etc. On a global scale, fluoride is one of the most prevalent ions in groundwater and is a threat to health, especially in China, India, Kenya, Nigeria, South America (Andes and Western Brazil), Northwestern Iran, Sri Lanka and Pakistan [4,5].

In groundwater, the natural concentration of fluoride depends on the geological, chemical and physical characteristics of the aquifer, the porosity and acidity of the soil and rocks, the temperature, the action of other chemical elements, and the depth of wells [6]. As reported by the World Health Organization (WHO), fluoride can be beneficial to living entities if its concentration is lower than 1.5 mg L^{-1}. But consumption of water containing fluoride at 1.5 mg L^{-1} causes diseases such as fluorosis, arthritis, hip fractures, infertility, osteoporosis and polydipsia. It affects the teeth and skeleton, and accumulation of fluoride over a long period of time can even lead to changes in DNA structure [7,8]. In several regions of Morocco, fluoride levels exceed acceptable standards, for instance in the Benguerir plateau (Central Morocco). Water in this region generally exceeds fluoride standards. This contamination is due to the phosphate deposit [9]. The National Office of Electricity and Potable Water (ONEE) has until now proceeded dilution to avoid frequent seasonal excesses of fluoride. The decline in water resources, particularly underground water, and the frequent excesses of fluoride observed in recent decades, make this solution unsustainable in the long-term. Therefore, to avoid this situation, ONEE has launched studies to examine remediation options. Due to the high solubility of fluorides in water, defluorination is a difficult and costly process [10].

A number of methods have been developed to remove excess fluoride from drinking water, such as the use of ion-exchange [11], precipitation [12], adsorption [13,14] and membrane-based processes [9,15–17]. However, the high investment required due to the energy needs of desalination limits its application to undeveloped/developed countries/communities. Therefore, recently, researchers have focused on other technologies with lower energy requirements. Membrane filtration is one such technology for defluorination of brackish groundwater. The membrane serves as a selective barrier that allows only certain size-specific constituents to cross membrane, while other large-size constituents are retained by membrane in the concentrate [18–20].

Various studies on fluoride removal have been reported. Tahaikt et al. [16], studied fluoride removal from water with three commercial membranes with different configurations. The obtained fluoride rejection varied with initial fluoride content but exceeded 74% for NF270 and TR60. For NF90, which is less sensitive to initial fluoride concentration, fluoride rejection exceeded 98%. Elazhar et al. [21], employed spiral-type membranes (NF90 8040) to remove fluoride ions in optimized conditions and obtained a fluoride rejection of 97.8% corresponding to water recovery of 84% and a pump pressure of 10 bar. Mnif et al. [22], investigated the defluorination of aqueous solutions using a thin film composite polyamide nanofiltration (NF) membrane called HL 2514 T manufactured by Osmonics (USA). The results showed that fluoride rejection by the HL membrane exceeds 80%. Nasr et al. [23], studied the commercial NF membranes NF5 and NF9 (manufactured by Applied Membranes USA) to removing fluoride ions from Tunisian groundwater. NF9 exhibited a better rejection (88%) than NF5 (57%). The amounts of total dissolved solids observed in the permeate were low (0.45 mg L^{-1}). Consequently, remineralization is required to rebalance the water. Chakrabortty et al. [24], studied defluorination of groundwater contaminated with fluoride in some areas in eastern India using the composite polyamide nanofiltration membrane used in crossflow mode was not only successful in removing 98% fluoride from contaminated water but also reduced the high pH of 10.01 for a volumetric crossflow rate of 750 L h^{-1} of the water to the desired level while yielding a high flux of 158 L h^{-1} m^{-2}. Pontié et al. [25], employed a NF45, polyamide NF membrane (FilmTec), a fluoride rejection of 91% was achieved for NaF concentration in the feed of 0.02 M.

The development of mathematical models for the prediction of membrane separation processes is a valuable tool in the field of science and technology [26]. There are two ways in which mathematical models can be handled. The first approach is the theoretical approach, where models are developed on the basis of existing knowledge. The second is the empirical approach, which is not based on any knowledge of the fundamental principles of the process [27]. A statistical tool is used to design experiments and develop models, the response surface methodology (RSM), could be used to conduct a set of statistically suggested experiments and find the optimal values of independent parameters [28–32]. Alka et al. [33], used predictive models based on machine learning techniques such as RSM and ANN (artificial neural network) to predict the permeate flow, water recovery, salt rejection and specific energy consumption of reverse osmosis (RO) and NF pilot plants, in order to optimize and compare RO and NF for better performance. Jadhav et al. [34] studied the removal of multiple contaminants such as fluoride, arsenic, sulphate and nitrate. The central composite design was applied. The mean rejection observed for NF90 was 95%, 98%, 87%, and 76% for sulfate, arsenic, fluoride and nitrate respectively, while NF270 rejected 90%, 94%, 57%, and 60%, respectively.

The aim of this study is to compare and evaluate the performance of three NF membranes in fluoride removal in continuous mode. Two complementary methodologies will be employed. The first is the determination of the effect of fluoride concentration in the feed and transmembrane pressure on fluoride rejection. The second is the optimization for better performance using RSM models by minimizing the permeate concentration and maximizing fluoride rejection and permeate flux.

2. Experimental

2.1. Characteristics of the feed water

The experiments are conducted on groundwater doped by NaF at different concentrations. The analytical results of the feed water are presented in Table 1.

2.2. Unit pilot testing

The experiments are performed on an NF/RO pilot plant (E 3039) supplied by TIA Company (Technologies

Industrielles Appliquées, France) shown in Fig. 1. The applied transmembrane pressure (TMP) can be varied from 5 to 70 bar with manual valves.

The pilot plant is equipped with two identical pressure vessels operating in series. Each pressure vessel contains one element. The pressure loss is about 2 bar corresponding to 1 bar of each pressure vessel. The two spiral wound modules are equipped with two identical commercial membranes.

The temperature is kept at 29°C using the heat exchanger. Samples of permeate are collected and water parameters are determined analytically following standard methods previously described [9,15,16]. Some other parameters are as follows:

- Flux of the permeate is given by the equation [37–39].

$$J_v = \frac{Q_p}{S}\left(\frac{L}{m^2 \cdot s} \text{ or } \frac{m^3}{m^2 \cdot s}\right) \quad (1)$$

where S is the membrane surface area (m^2) and Q_P is the flow rate of the permeate (L h^{-1} or m^3 s^{-1}).

- The recovery rate (Y) is defined as:

$$Y(\%) = \frac{Q_p}{Q_0} \times 100 \quad (2)$$

where Q_P is the permeate flow (L h^{-1}) and Q_0 is the feed flow (L h^{-1}).

- Salt rejection (R) is defined as:

$$R = \left(1 - \frac{C_p}{C_0}\right) \times 100 \quad (3)$$

where C_P is the solute concentration in permeate (g L^{-1}) and C_0 is the solute concentration in the feed water (g L^{-1}).

2.3. Characteristics of the membranes

The two spiral wound modules are equipped with two identical commercial NF membranes. Table 2 gives the characteristics of the membranes used. After the run, the membranes are cleaned with alkaline and acidic cleaning solutions according to the manufacturer's recommendations.

Table 1
Characteristics of the feed water

Parameter	Feed water	Moroccan guidelines [35]	WHO standards [36]
Temperature (°C)	29	–	–
Turbidity, NTU	<2	–	–
pH	7.41	6–9.2	6.5–8.5
pHs	7.80	–	–
Conductivity, μs cm^{-1}	1,492	2,700	–
Hardness, mg L^{-1} $CaCO_3$	440	500	500
Alkalinity, mg L^{-1} $CaCO_3$	320	200	–
Fluoride, mg L^{-1}	1-2-3-5-7-10-15-20	1.5	1.5
Sulphate, mg L^{-1}	116	200	200
Nitrate, mg L^{-1}	20	50	50
Chloride, mg L^{-1}	560	750	250

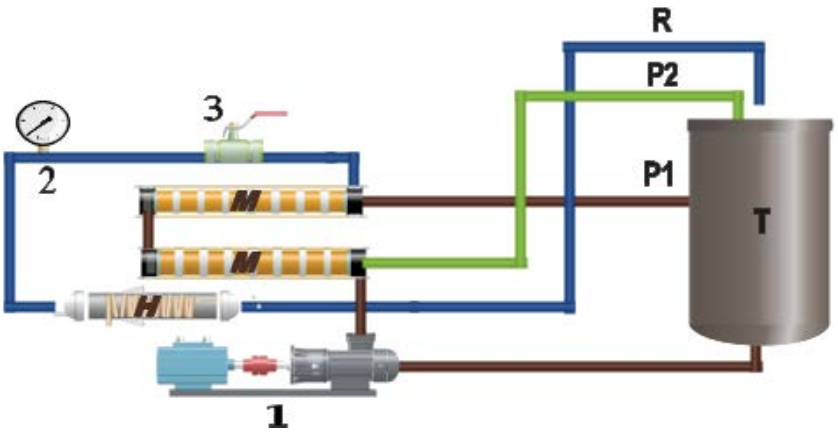

Fig. 1. Schematic diagram of the nanofiltration/reverse osmosis pilot plant. T: tank; M: nanofiltration module; P: permeate recirculation; R: retentate recirculation; H: heat exchanger; 1: high-pressure pump; 2: pressure sensor. 3: pressure regulation valves.

Table 2
Characteristics of the membranes used

Membrane	Surface (m^2)	Material	Manufacturer
NF90 40 × 40	7.6	Polyamide	FilmTec Dow (USA)
NF270 40 × 40	7.6	Polyamide	FilmTec Dow (USA)
TR60 40 × 40	6.8	Polyamide	Toray (Japan)

2.4. Optimization of NF module by RSM

The experimental design of fluoride removal is carried out using RSM. In this present study, the central composite design (CCD), which is a well-exploited model of RSM, is used to optimising fluoride removal by NF. For the NF process, significant variables, such as TMP and initial fluoride concentration in the feed, are chosen as the independent variables and designated as X_1, X_2 respectively. The experiments are carried out for the factors and range, as shown in Table 3.

The design matrix obtained after the application of CCD is mentioned in Table 4.

The results are subjected to analysis of variance (ANOVA) using RSM modelling software (Design-Expert).

CCD for studying the removal process, with two input variables, consists of 13 experiments with 4 (2^k) orthogonal two-level full-factorial design points (coded as ±1), 4 (2^k) axial points (or star point coded as $\pm\alpha = 1.41$) and 5 replications of the central points to provide an estimation of the experimental error variance. The performance of each NF is assessed in terms of final permeate concentration (Y_1), fluoride rejection (Y_2) and the permeate flux (Y_3) which are considered as responses. The following polynomial equation describes the predicted values of the responses Y_1, Y_2 and Y_3 as:

$$Y_1, Y_2 \text{ and } Y_3 = \beta_0 + \sum_{i=1}^{2}\beta_i X_i + \sum_{i=1}^{2}\sum_{j=1}^{2}\beta_{ij} X_i X_j + \sum_{i=1}^{2}\beta_{ii} X_i^{\,2} + \xi \qquad (4)$$

where Y_1, Y_2 and Y_3 are the predicted response, β_0 is the constant coefficient, β_i is the linear coefficients, β_{ij} is the interaction coefficients, β_{ii} is the quadratic coefficients, and X_i and X_j are the coded values of the fluoride NF variables and ξ is the residual term.

3. Results and discussion

3.1. Effect of TMP and initial fluoride concentration in the feed

3.1.1. Effect of TMP

The transmembrane pressure effect on the physico-chemical quality of the permeate was studied in batch mode. Fig. 2 shows the variation of permeate flux, electric conductivity, pH, alkalinity, hardness and nitrate, sulfate and chloride contents as a function of TMP. Knowing that these values are almost the same as those obtained for the different feed solutions tested, except for fluoride ions.

The permeate flux (Fig. 2A) increases almost linearly with operating TMP according to Darcy's law for the three membranes. Increased TMP overcomes membrane resistance. In this illustration, NF270 shows the maximum flux, followed by TR60 and NF90. This means that NF90 is the tightest of these membranes while NF270 is the loosest.

Table 3
Independent input variables range in terms of coded levels

Factors	Coded level				
	−α	−1	0	+1	+α
Initial fluoride concentration in the feed (mg L^{-1}):TR60-NF270-NF90	0.51	3	9	15	17.48
TMP (bar):TR60	3.96	5	7.5	10	11.03
TMP (bar):NF270	2.92	5	10	15	17.07
TMP (bar):NF90	4.82	10	22.5	35	40.177

For NF90, the permeate conductivity (Fig. 2B) is very low and decreases slightly with increasing TMP. For TR60 the permeate conductivity decreases with increasing TMP, similarly for NF270, the conductivity decreases to a minimum at a TMP of 10 bar, beyond this value a slight increase in conductivity was observed, which shows that hydraulic phenomena that take precedence over selectivity, hence the increase in conductivity. At a TMP of 7 bar, the same water quality in terms of conductivity was observed for both TR60 and NF270 membranes.

For the three membranes, a decrease in the nitrate concentration (Fig. 2C) was observed for the different TMPs, with the exception of NF270 which begins to lose its selectivity beyond 10 bars and its nitrate concentration increases in the permeate. The nitrate concentration in the permeate followed the sequence below TR60 > NF270 > NF90.

A little variation in pH is observed (Fig. 2D) for all the membranes pH values found for TR60 and NF270 are higher than of NF90. This behaviour is determined by the ratio of CO_2/HCO_3^- in the feed and in the permeate. The three membranes are crossed by CO_2, but rejection of HCO_3^- by NF90 is more significant than with TR60 and NF270. This difference is responsible for the lower pH of the permeate for NF90 according to the relationship (5) [38]:

$$pH = pK_1 - \varepsilon + \log\left[HCO_3^-\right] - \log\left[CO_2\right] \qquad (5)$$

where ε is expressed as a function of the ionic strength, μ of the solution $\varepsilon = \frac{\sqrt{\mu}}{1+\sqrt{\mu}}$, and pK_1 is the acidity constants of carbonic acid.

A significant reduction (Fig. 2E and F) in the concentrations of sulfate and chloride ions is observed for the two membranes TR60 and NF270, and the cencentration of these ions decrease with increasing TMP, however, for NF270, and the concentrations of these ions begin to increase beyond 10 bar. For the NF90 membrane, these ions are greatly reduced over the entire TMP range with removal rates of 98% and 100% respectively.

The alkalinity and hardness (Fig. 2G and H) of the permeate obtained with TR60 and NF270 are satisfactory at different TMPs applied. On the other hand, For the NF90 membrane, the alkalinity and hardness are very low.

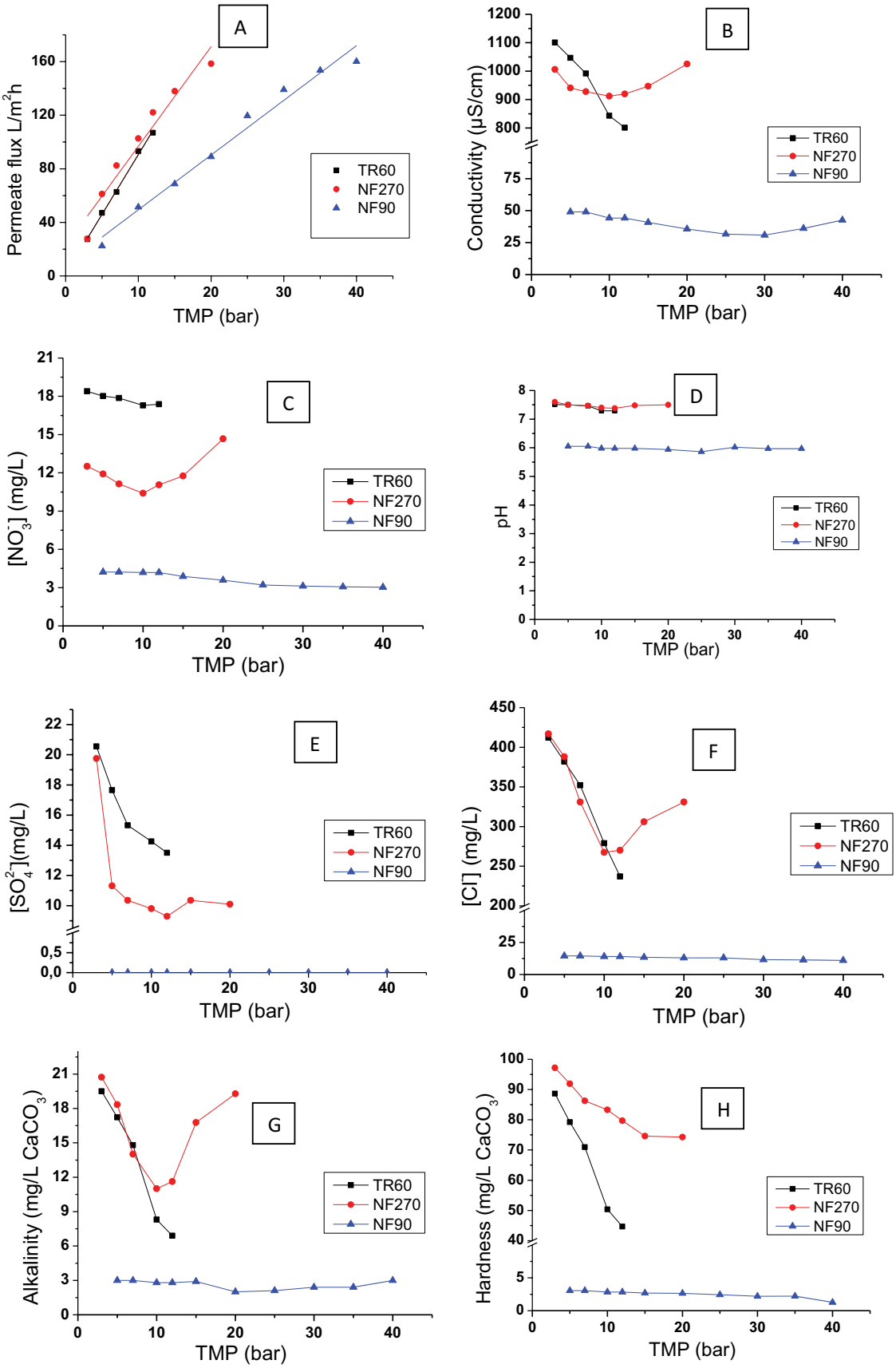

Fig. 2. Permeate characteristics as a function of operating TMP.

In general, for TR60 and NF90, the ion content decreases with the TMP applied over the entire pressure range studied. For NF270, the ion content decreases with the TMP applied as long as the pressure is below 10 bar. The ions content obtained with NF90 is lower than that obtained with TR60 and NF270. This outcome can be explained by the structure of the NF90 membrane which is close to that of RO membranes and also the dominant mode of salt transport through these membranes is diffusion [40].

In NF, the rejection is due to the hydration energy of ions and the surface and drag force. In addition, and according to Nghiem et al. [41], the measurements of the contact angle with water for the NF270 and NF90 are (55°, 42.5°) respectively indicate that the two membranes are relatively hydrophobic [41,42], the zeta potentials of these two membranes were slightly positive below pH 3.5 and are negatively charged above this pH, due to the deprotonation of the functional groups [41,43] which explains the excellent performance of these two membranes [44]. The same thing can be said about the TR60 membrane since it too is made of the same materials. At high TMP, the drag force will prevail and give low rejection [45,46].

Thus, the physico-chemical quality of the water obtained is satisfactory for NF270 and TR60. For NF90, water is strongly demineralised and requires remineralisation. This result is consistent with a study of a similar treatment [47].

3.1.2. Effect of initial fluoride concentration in the feed on fluoride rejection

The effect of the initial fluoride concentration in the feed on fluoride rejection at different operating TMP is illustrated in Fig. 3 for the three membranes.

When initial fluoride concentration in the feed increases, fluoride rejection increases slightly (Figs. 3A–C) and then reaches a plateau for different operating TMP for the three membranes. This behaviour is in accordance with the Donnan exclusion model [48].

For the applied TMP range the fluoride rejection exhibited by NF90 is higher than those obtained by TR60 and NF270 according to the following sequence:

$$R_{NF90} > R_{TR60} > R_{NF270}$$

The high rejection of the fluoride ion in NF membranes is attributed mostly to the steric and charge effects as well to its very small size and more highly hydrated shell, its high charge density [49], to elevated pH which would change the membrane surface charge to negative form according to deprotonation of carboxyl functional groups ($COOH \rightarrow COO^-$) [50], to the Donnan classical equilibrium, and to the membrane charge neutralization effect due to the cation concentration [49].

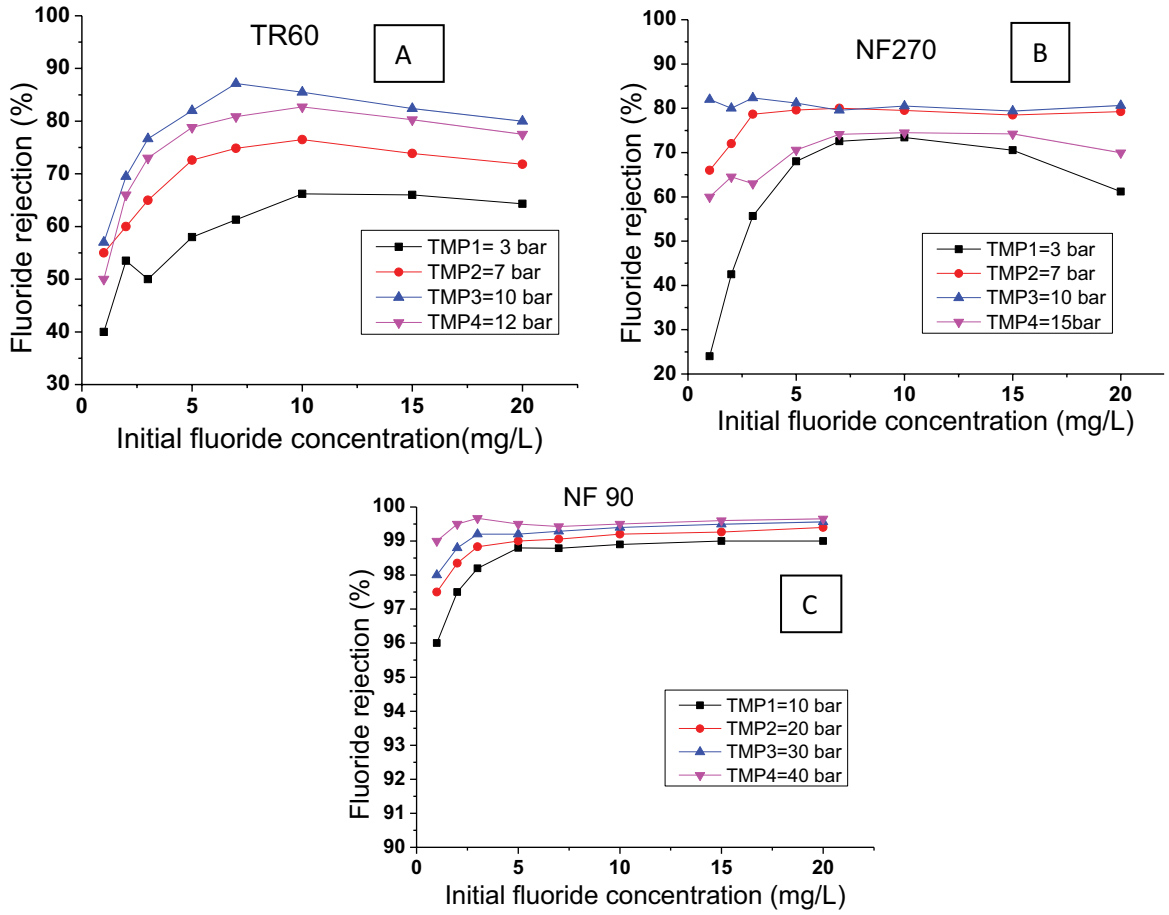

Fig. 3. Fluoride rejection vs. initial fluoride concentration in the feed.

From the previous figures, we have found that fluoride rejection is influenced by the initial fluoride concentration in the feed and likely by operating TMP for all the three membranes. To confirm or deny this hypothesis, we adopt an RSM approach based on CCD.

3.2. Statistical analysis and modelling by RSM

3.2.1. Experimental process performance

The process responses investigated for the model are permeate concentration, fluoride rejection and permeate flux. The experimental design and results for the modelling are shown in Table 4. Table 5 represents the ANOVA models developed for the responses of TR60, NF270 and NF90 membranes. The statistical analysis indicates that *P*-values less than 0.0500 indicate model terms are significant. Values greater than 0.1000 indicate the model terms are not significant. If there are many insignificant model terms (not counting those required to support hierarchy), model reduction may improve your model. The *F*-values of the models imply that the models are significant. There is only a small chance that such a high *F*-value is due to noise.

The regression equations for permeate concentration generated for TR60, NF270 and NF90 are Eqs. (6)–(8), respectively.

$$Y_1 = -0.813914 + 0.383461X_1 + 0.279808X_2 - 0.020000X_1X_2 - 0.025800X_1^2 + 0.007049X_2^2 \quad (6)$$

$$Y_1 = +0.039096 - 0.001599X_1 + 0.010285X_2 - 0.000143X_1X_2 + 0.000022X_1^2 - 0.000094X_2^2 \quad (7)$$

$$Y_1 = +2.82089 - 0.500373X_1 + 0.115176X_2 + 0.004083X_1X_2 + 0.023700X_1^2 + 0.003194X_2^2 \quad (8)$$

The regression equations for fluoride rejection generated for TR60, NF270 and NF90 are Eqs. (9)–(11), respectively.

$$Y_1 = +42.50729 + 0.485391X_1 + 4.52497X_2 - 0.088667X_1X_2 + 0.163200X_1^2 - 0.167500X_2^2 \quad (9)$$

$$Y_1 = +6.22187 + 5.13522X_1 + 8.43217X_2 - 0.136167X_1X_2 - 0.176475X_1^2 - 0.284705X_2^2 \quad (10)$$

$$Y_1 = +96.88400 + 0.048940X_1 + 0.283158X_2 - 0.002533X_1X_2 - 0.000040X_1^2 - 0.008646X_2^2 \quad (11)$$

The regression equations for permeate flux generated for TR60, NF270 and NF90 are Eqs. (12)–(14), respectively.

$$Y_1 = +61.69397 - 8.54561X_1 - 0.037604X_2 + 0.000083X_1X_2 + 1.15920X_1^2 + 0.002049X_2^2 \quad (12)$$

$$Y_1 = +1.69253 + 11.93403X_1 - 0.210625X_2 - 7.24685E-16X_1X_2 - 0.173950X_1^2 + 0.011701X_2^2 \quad (13)$$

$$Y_1 = -19.91611 + 8.25635X_1 + 0.359807X_2 - 1.42479E-16X_1X_2 - 0.094817X_1^2 - 0.019984X_2^2 \quad (14)$$

The R^2 (correlation coefficient-squared) is also computed for the model which describes the variability and accuracy of the generated models. R^2 is computed for permeate concentration, fluoride rejection and permeate flux respectively for TR60, NF270 and NF90 as shown in Table 5. The values of R^2 closer to 1 indicate towards a better prediction of response using the model. The adaptability of the generated

Table 4
CCD for the two independent variables

Run	Coded variables values		Responses values								
			TR60			NF270			NF90		
	X_1	X_2	Y_1	Y_2	Y_3	Y_1	Y_2	Y_3	Y_1	Y_2	Y_3
1	0	0	2.35	76.50	62.64	1.95	80.5	102.69	0.07	99.3	119.47
2	0	0	2.35	76.50	62.64	1.95	80.5	102.69	0.07	99.3	119.47
3	–1	1	4.34	71.06	47.05	3.87	74.2	62.25	0.15	99	51.44
4	1	–1	0.7	76.66	93.16	1.11	63	137.96	0.015	99.5	153.55
5	0	0	2.35	76.50	62.64	1.95	80.5	102.69	0.07	99.3	119.47
6	–α	0	2.77	72.30	47.05	2.66	73.4	27.82	0.1	99	22.43
7	0	0	2.35	76.50	62.64	1.95	80.5	102.69	0.07	99.3	119.47
8	0	α	5.64	71.80	62.64	3.87	80.65	102.69	0.1	99.5	119.47
9	α	0	1.73	82.70	106.91	3.3	67	158.48	0.05	99.42	160.13
10	1	1	2.64	82.40	93.16	3.87	74.2	137.96	0.068	99.54	153.55
11	0	0	2.35	76.50	62.64	1.95	80.5	102.69	0.07	99.3	119.47
12	0	–α	0.45	55	62.64	0.18	42	102.69	0.023	97.7	119.47
13	–1	–1	1.2	60	47.05	1.6	46.66	61.25	0.054	98.2	51.44

Table 5
ANOVA for the three models, permeate concentration, fluoride rejection, permeate flux of TR60, NF270 and NF90

Model	Response	Sum of squares	Degree of freedom	Mean square	*F*-value	*P*-value	R^2	R^2_{adj}
TR60	Permeate concentration	20.97	5	10.48	50.30	<0.0001	0.9536	0.9204
	Fluoride rejection	716.74	5	143.35	27.27	0.0002	0.9512	0.9163
	Permeate flux	4,280.57	5	856.11	817.35	<0.0001	0.9983	0.9971
NF270	Permeate concentration	14.55	5	2.91	116.47	<0.0001	0.9881	0.9796
	Fluoride rejection	1,983.79	5	396.76	33.12	<0.0001	0.9594	0.9305
	Permeate flux	14,435.98	5	2,887.20	157.13	<0.0001	0.9912	0.9849
NF90	Permeate concentration	0.0136	5	0.0027	35.03	<0.0001	0.9616	0.9341
	Fluoride rejection	3.00	5	0.6000	6.93	0.0122	0.8320	0.7120
	Permeate flux	21,433.15	5	4,286.63	1,077.90	<0.0001	0.9987	0.9978

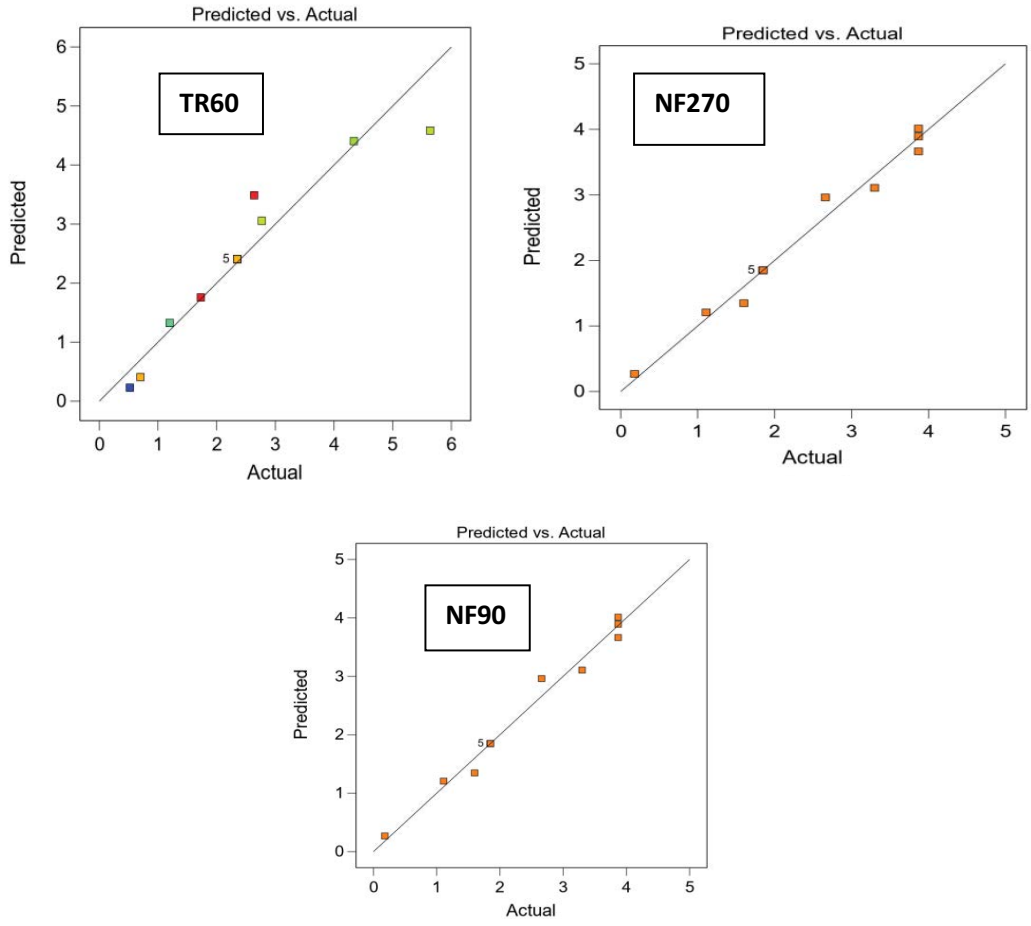

Fig. 4. Predicted vs. actual values for permeate concentration.

model is confirmed by the adjusted R^2 (R^2_{adj}) which is close to the corresponding R^2 value. The predicted and experimental values are plotted, as shown in Figs. 4–6.

Fig. 4 compares the experimental values for permeate concentration to the predicted data calculated by applying the regression equations [Eqs. (6)–(8)] for the three membranes.

Fig. 5 compares the experimental rejection values of fluoride ions to the predicted data calculated by applying the regression equations [Eqs. (9)–(11)] for three membranes.

Fig. 6 compares the experimental data of the permeate flux values to the predicted data calculated by applying the regression equations [Eqs. (12)–(14)] for three membranes.

These graphics reveal that the model-predicted values are in accordance with the experimental values for the range studied. The coefficient of correlation is determined by the *R*-value. In Table 5 it can be seen that for all the membranes, the *R*-value is closer to unity, which demonstrates a positive relationship between the data.

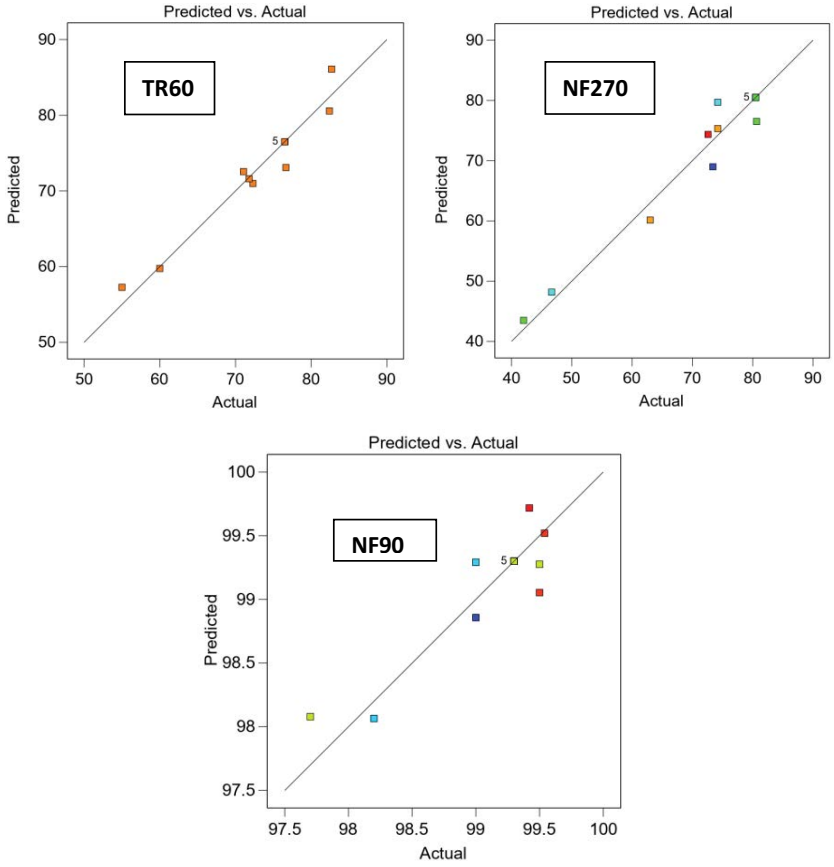

Fig. 5. Predicted vs. actual values for fluoride rejection.

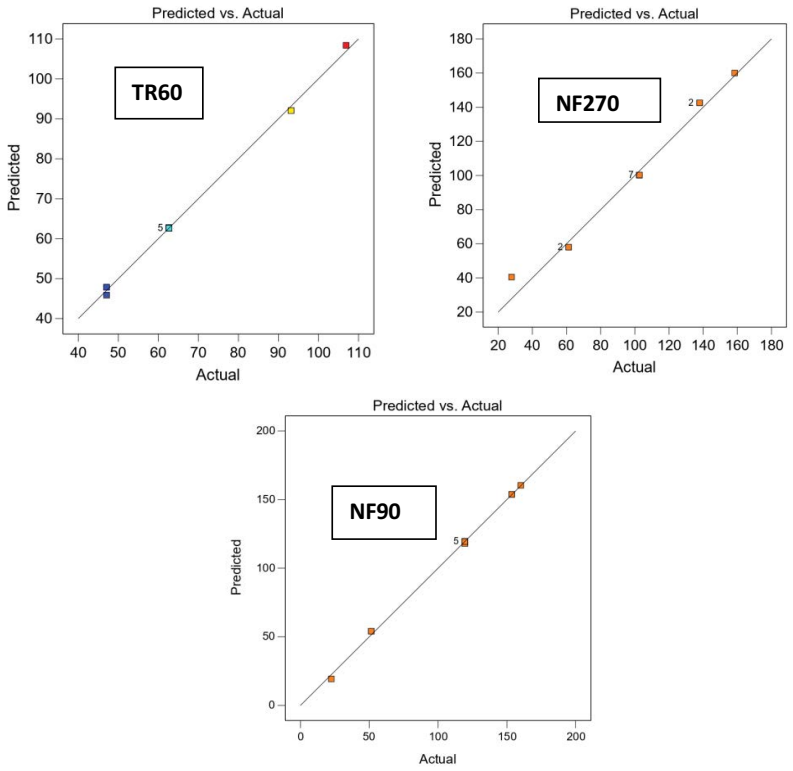

Fig. 6. Predicted vs. actual values for permeate flux.

3.2.2. Permeate concentration

Fig. 7 shows the response surface graphs effect of TMP and initial fluoride concentration in the feed on permeate concentration. The 3D response surface allows the interaction of these parameters to be visualized.

The ANOVA results indicate a significant effect of initial fluoride concentration in the feed on permeate concentration for both TR60 and NF270. There is also a significant interaction effect between operating TMP and initial fluoride concentration in the feed on permeate concentration for NF90.

Fig. 7 shows the response surface for both TR60, NF270 that the permeate concentration increases significantly with increasing initial fluoride concentration in the feed, however, the effect of TMP turns out to be insignificant. Thus, high fluoride concentration in the permeate that exceeding standards (>1.5 mg L^{-1}) are observed.

Note that the optimum values obtained are an initial fluoride concentration in the feed of 7 and 5.5 mg L^{-1}, and a TMP of 10 and 13 bar for TR60 and NF270 respectively.

A significant increase of permeate concentration in the permeate with increasing interaction of initial fluoride concentration in the feed and TMP for NF90. The range of permeate concentration obtained remains lower than the standard. In this case, the effect of initial fluoride concentration in the feed and TMP is negligible.

These results can be compared with the experiments carried out by Jadhav et al. [34] on NF90 and NF270 to removing fluoride. In this research, results showed that varying the initial fluoride concentration in the feed from 10 to 20 mg L^{-1} (0.1–0.2 kg m^{-3}) results in permeate fluoride concentration below the WHO limit 1.5 mg L^{-1}.

3.2.3. Fluoride rejection

Fig. 8 shows the response surface graphs effect of TMP and initial fluoride concentration in the feed on fluoride rejection. The 3D response surface allows the interaction of these parameters to be visualized.

The ANOVA results indicate a significant effect of initial fluoride concentration in the feed on fluoride rejection for TR60 and NF270, and for NF90 a significant effect of initial fluoride concentration in the feed on fluoride rejection with a less significant effect of TMP.

For TR60 and NF270, the initial fluoride concentration in the feed (Fig. 8) appears to affect the fluoride rejection. Also, TMP seems to affect the fluoride rejection more at higher initial fluoride concentration than the lower end.

The fluoride rejection is relatively stable with increasing TMP. The optimal conditions that give the maximum fluoride rejection predicted by the model are illustrated in Table 6. Previous one-factor-at-a-time studies showed that TMP alone had a small effect on the rejection rate. For example, Huang, et al. [50], examined rejection rate under TMP of 40–800 kPa and concluded that TMP did not significantly affect the rejection rate. Mnif et al. [22], have reported similar conclusions for a TMP range of 3–20 bar and concluded that at higher TMP, fluoride rejection is practically unaffected. This may reflect the fact that TMP primarily provides a driving force for mass transport across the membrane and will not affect the interactions between ions and membrane. While for NF90, both parameters slightly affect the rejection.

3.2.4. Permeate flux

Fig. 9 shows the response surface graphs effect of TMP and initial fluoride concentration in the feed on permeate flux. The 3D response surface allows the interaction of these parameters to be visualized.

The ANOVA results indicate a significant effect of TMP on permeate flux for all three membranes.

In Fig. 9 the response surface indicates that an increase in TMP is increasing the permeate flux. The permeate flux increases gradually in the lower ranges and increases rapidly in the upper ranges for the three membranes. The permeate flux of the NF270 is much higher than that of the TR60 and NF90. This is due to the pore size of the membranes which limits the permeate flux [50,51].

3.3. Optimisation and prediction of modelling using RSM

Process optimization for permeate concentration (mg L^{-1}), fluoride rejection and permeate flux (L h^{-1} m^{-2}) are calculated by RSM model. As mentioned previously, three separate predictive models are presented for the response functions for each NF membrane studied. The fluoride ions removal process aims at minimizing permeate concentration and at treating large volumes of water maximize permeate flux, as well as fluoride rejection for TR60 and NF270. While for NF90, the permeate concentration is low in reality, so the process maximizes permeate concentration.

The optimal conditions of the fluoride ions removal are obtained using the desirability function approach in Design Expert.

The optimum conditions of TR60, NF270 and NF90 membranes are shown in Table 6.

4. Conclusion

This research work deals with removal of fluoride ions by NF performed on groundwater doped with NaF using three membranes. The experimental results show that in the range of studied operating TMP, rejection of fluoride ions by NF90 is higher than those obtained by TR60 and NF270 which are almost similar. This fluoride rejection follows the following order:

$$R_{NF90} > R_{TR60} > R_{NF270}$$

Furthermore, RSM, shown in the central composite design, is one of the appropriate methods to optimize the operating conditions minimizing the permeate concentration and maximizing the fluoride rejection and permeate flux for TR60 and NF270. The analysis of variance shows a high value of the coefficient of determination ($R^2 > 0.90$), thus ensuring a satisfactory fit of the second-order regression model with the experimental data. The optimization of the models allows to obtain the optimal conditions at an initial fluoride concentration in the feed of 7 and 5.5 mg L^{-1}, at operating TMP of 10 and 13 bar respectively. The graphical response surface and contour lines are used to locate

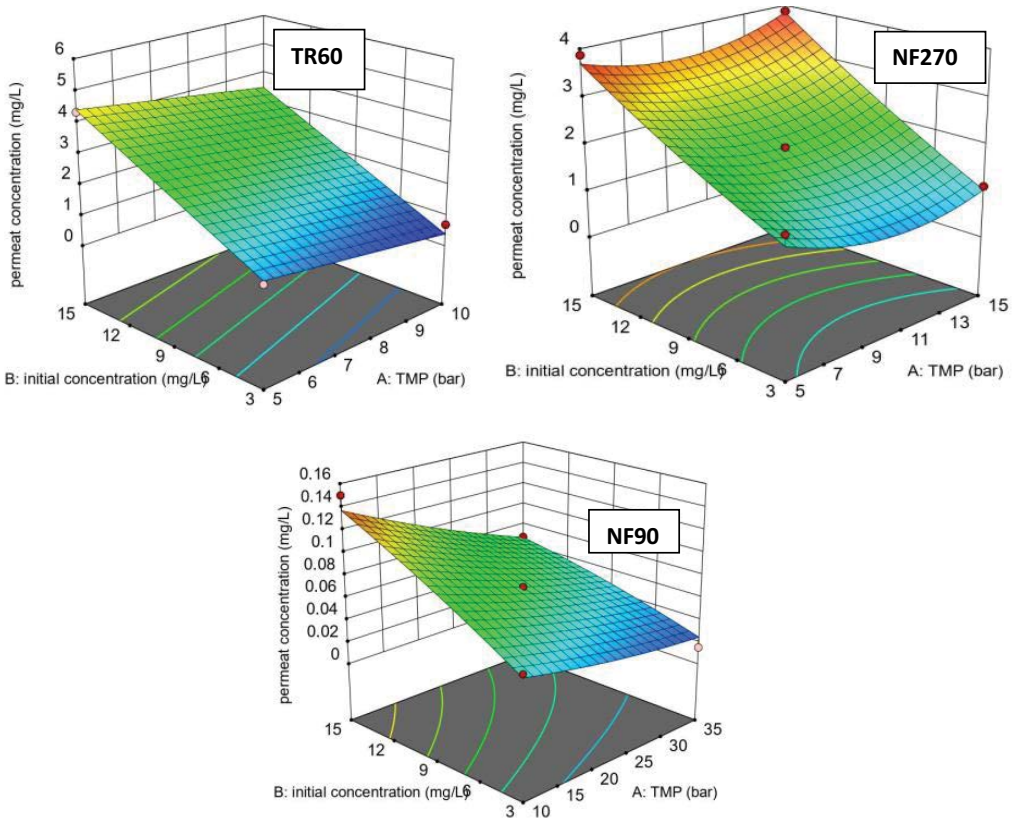

Fig. 7. Response surface plot for permeate concentration.

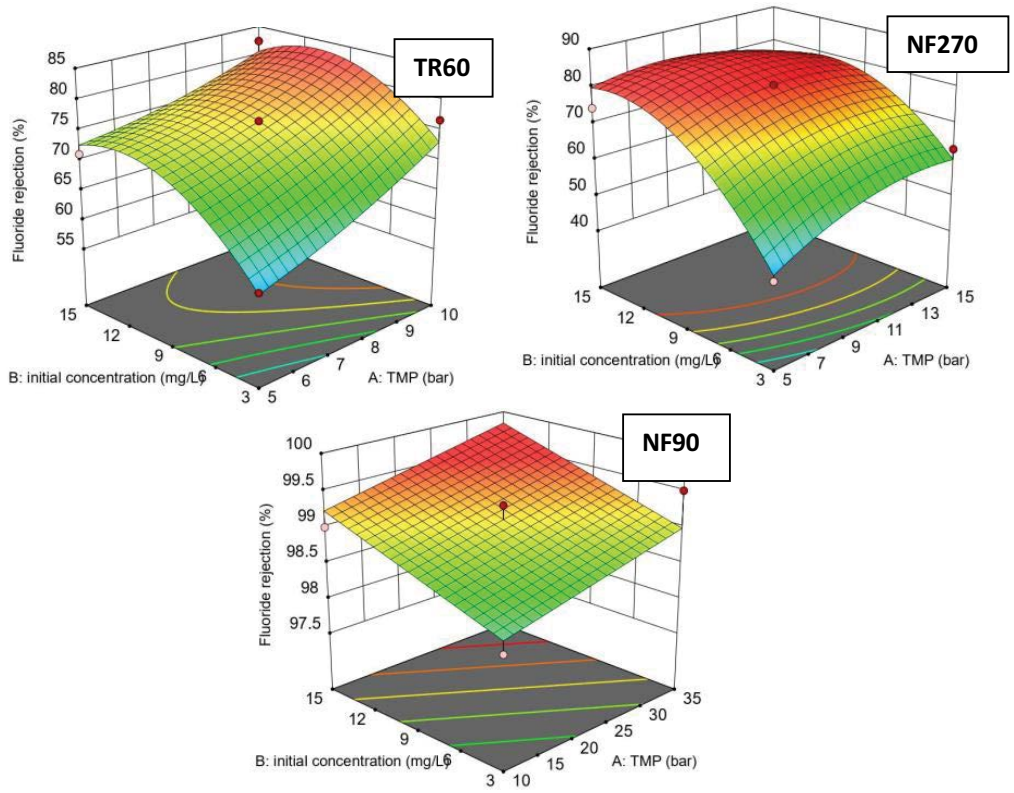

Fig. 8. Response surface plot for fluoride rejection.

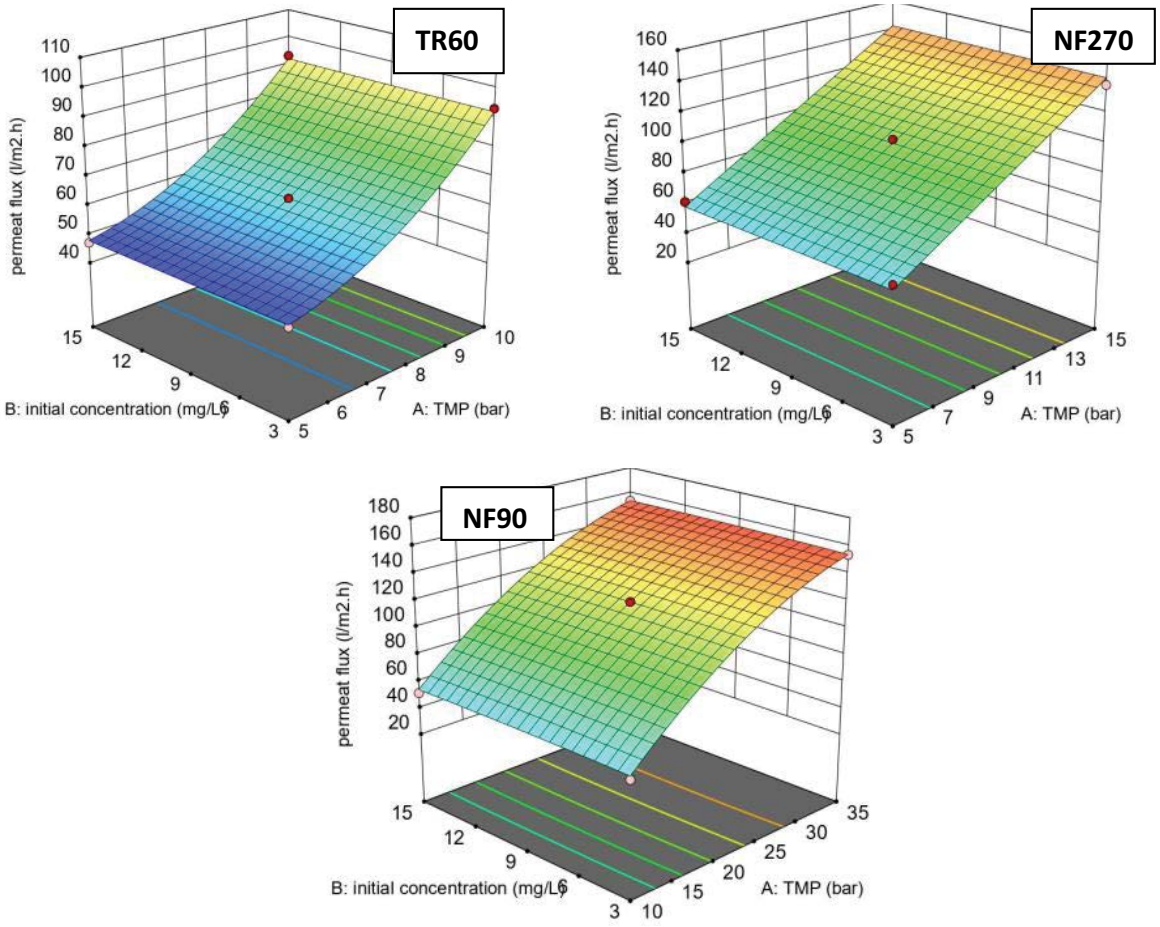

Fig. 9. Response surface plot for permeate flux.

Table 6
Response optimisation by RSM

	TR60	NF270	NF90
Optimum input variables			
TMP (bar)	10	13	10
Initial fluoride concentration in the feed (mg L^{-1})	7	5.5	3
Predicted responses by RSM			
Permeate concentration (mg L^{-1})	1.5	1.5	0.1
Fluoride rejection (%)	79.694	72.022	98.75
Permeate flux (L h^{-1} m^{-2})	86.228	133.936	57
Desirability	0.856	0.834	1

the optimum point. For NF90, we try to maximize the permeate concentration despite the fact that it is very low compared to the standards fixed by WHO.

References

[1] W.M. Edmunds, P.L. Smedley, Fluoride in Natural Waters, O. Selinus, Ed., Essentials of Medical Geology, Springer, Dordrecht, 2013, pp. 311–336.
[2] WHO/UNICEF, Progress on Drinking Water and Sanitation, 2014 Update (WHO, Geneva, 2012).
[3] M. Mohapatra, S. Anand, B.K. Mishra, D.E. Giles, P. Singh, Review of fluoride removal from drinking water, J. Environ. Manage., 91 (2009) 67–77.
[4] A. Elhalil, S. Qourzal, F.Z. Mahjoubi, R. Elmoubarki, M. Farnane, H.Tounsadi, M. Sadiq, M. Abdennouri, N. Barka, Defluoridation of groundwater by calcined Mg/Al layered double hydroxide, Emerging Contam., 2 (2016) 42–48.
[5] R. Dhanya, E. Shaji, Fluoride contamination in groundwater resources of Alleppey, Southern India, Geosci. Front., 8 (2017) 117–124.
[6] M.M. Emamjomeh, M. Sivakumar, An empirical model for defluoridation by batch monopolar electrocoagulation/flotation (ECF) process, J. Hazard. Mater., 131 (2006) 118–125.
[7] P. Senthil Kumar, S. Suganya, S. Srinivas, S. Priyadharshini, M. Karthika, R. Karishma Sri, V. Swetha, Mu. Naushad, E. Lichtfouse, Treatment of fuoride contaminated water. A review, Environ. Chem. Lett., 17 (2019) 1707–1726.
[8] S. Water, World Health Organization Guidelines for Drinking-Water Quality [Electronic Resource]: Incorporating First Addendum, World Health Organization, 2006, pp. 375–377.
[9] M. Tahaikt, R. El Habbani, A. Ait Haddou, I. Achary, Z. Amor, M. Taky, A. Alami, A. Boughriba, M. Hafsi, A. Elmidaoui, Fluoride removal from groundwater by nanofiltration, Desalination, 212 (2007) 46–53.
[10] M. Bodzek, K. Konieczny, Removal of fluoride from aquatic environment, Desal. Water Treat., 117 (2018) 118–141.
[11] B. Solangi, S. Memon, M.I. Bhanger, An excellent fluoride sorption behavior of modified amberlite resin, J. Hazard. Mater., 176 (2010) 186–192.

[12] Meenakshi, R.C. Maheshwari, Fluoride in drinking water and its removal, J. Hazard. Mater., 137 (2006) 456–463.
[13] S.P. Kamble, P. Dixit, S.S. Rayalu, N.K. Labhsetwar, Defluoridation of drinking water using chemically modified bentonite clay, Desalination, 249 (2009) 687–693.
[14] M.A. Menkouchi Sahli, S. Annouarb, M. Tahaikt, M. Mountadar, A. Soufiane, A. Elmidaoui, Fluoride removal for underground brackish water by adsorption on the natural chitosan and by electrodialysis, Desalination, 212 (2007) 37–45.
[15] M. Tahaikt, I. Achary, M.A. Menkouchi Sahli, Z. Amor, M. Taky, A. Alami, A. Boughriba, M. Hafsi, A. Elmidaouia, Defluoridation of Moroccan groundwater by electrodialysis: continuous operation, Desalination, 189 (2006) 215–220.
[16] M. Tahaikt, A. Ait Haddou, R. El Habbani, Z. Amor, F. Elhannouni, M. Taky, M. Kharif, A. Boughriba, M. Hafsi, A. Elmidaoui, Comparison of the performances of three commercial membranes in fluoride removal by nanofiltration. Continuous operations, Desalination, 225 (2008) 209–219.
[17] L. Shen, L. Tian, J. Zuo, X. Zhang, S. Sun, Y. Wang, Developing high-performance thin-film composite forward osmosis membranes by various tertiary amine catalysts for desalination, Adv. Composites Hybrid Mater., 2 (2019) 51–69.
[18] A. Lhassani, M. Rumeau, D. Benjelloun, M. Pontie, Selective demineralization of water by nanofiltration application to the defluorination of brackish water, Water Res., 35 (2001) 3260–3264.
[19] Y. Zhang, J. Guo, G. Han, Y. Bai, Q. Ge, J. Ma, C.H. Lau, L. Shao, Molecularly soldered covalent organic frameworks for ultrafast precision sieving, Sci. Adv., 7 (2021) eabe8706, doi: 10.1126/sciadv.abe8706.
[20] H. Hu, F. Ding, H. Ding, J. Liu, M. Xiao, Y. Meng, L. Sun, Sulfonated poly(fluorenyl ether ketone)/Sulfonated α-zirconium phosphate nanocomposite membranes for proton exchange membrane fuel cells, Adv. Compos. Hybrid Mater., 3 (2020) 498–507.
[21] F. Elazhar, M. Tahaikt, A. Achatei, F. Elmidaoui, M. Taky, F. El Hannouni, I. Laaziz, M. El Amrani, A. Elmidaoui, S. Jariri, Economical evaluation of the fluoride removal by nanofiltration, Desalination, 249 (2009) 154–157.
[22] A. Mnif, M. Ben Sik Ali, B. Hamrouni, Effect of some physical and chemical parameters on fluoride removal by nanofiltration, Ionics, 16 (2010) 245–253.
[23] A.B. Nasr, C. Charcosset, R.B. Amar, K. Walha, Defluoridation of water by nanofiltration, J. Fluorine Chem., 150 (2013) 92–97.
[24] S. Chakrabortty, M. Roy, P. Pal, Removal of fluoride from contaminated groundwater by cross flow nanofiltration: transport modeling and economic evaluation, Desalination, 313 (2013) 115–124.
[25] M. Pontié, H. Buisson, C.K. Diawara, H. Essis-Tome, Studies of halide ions mass transfer in nanofiltration-application to selective defluorination of brackish drinking water, Desalination, 157 (2003) 127–134.
[26] M. Khayet, C. Cojocaru, M. Essalhi, Artificial neural network modeling and response surface methodology of desalination by reverse osmosis, J. Membr. Sci., 368 (2011) 202–214.
[27] A. Shahsavand, M.P. Chenar, Neural networks modeling of hollow fiber membrane processes, J. Membr. Sci., 297 (2007) 59–73.
[28] D. Dolar, K. Košutić, T. Strmecky, Hybrid processes for treatment of landfill leachate: coagulation/UF/NF-RO and adsorption/UF/NF-RO, Sep. Purif. Technol., 168 (2016) 39–46.
[29] P. Pal, S. Chakrabortty, L. Linnanen, A nanofiltration–coagulation integrated system for separation and stabilization of arsenic from groundwater, Sci. Total Environ., 476–477 (2014) 601–610.
[30] B. Tansel, N. Dizge, Multi objective performance analysis of nanofiltration, process to loading parameters by response surface approach, Desalination, 272 (2011) 164–169.
[31] V. Yadav, J. Ali, M.C. Garg, Biosorption of methylene blue dye from textile industry wastewater onto sugarcane bagasse: response surface modelling, isotherms, kinetic and thermodynamics modelling, J. Hazard. Toxic Radioact. Waste, 25 (2021) 04020067.
[32] A. Mohagheghian, N. Besharati-Givi, K. Godini, R. Dewil, M. Shirzad-Siboni, Photocatalytic reduction of Cr(VI) from aqueous solution by visible light/CuO-Kaolin: optimization and modeling of key parameters using central composite design (CCD), Sep. Sci. Technol., 56 (2020) 1253–1271.
[33] S. Alka, K. Aghilesh, N. Akhil, R. Shobha, A. Smriti, A. Jahangeer, S. Rajneesh, C.G. Manoj, Response surface methodology and artificial neural network modelling for the performance evaluation of pilot-scale hybrid nanofiltration (NF) and reverse osmosis (RO) membrane system for the treatment of brackish ground water, J. Environ. Manage., 278 (2021) 111497, doi: 10.1016/j.jenvman.2020.111497.
[34] S.V. Jadhav, K.V. Marathe, V.K. Rathod, A pilot scale concurrent removal of fluoride, arsenic, sulfate and nitrate by using nanofiltration: competing ion interaction and modelling approach, J. Water Process Eng. 13, (2016) 153–167.
[35] Guidelines for Drinking-Water Quality: Fourth Edition Incorporating the First Addendum, ISBN 978-92-4-154995-0.
[36] Moroccan Official Bulletin, Joint Orders No. 1275-01, 1276-01 and 1277-01 of 17th October 2002 Defining the Quality Norms of Surface Waters, Waters Destined for Irrigation and of Surface Waters Used for the Production of Drinking Water Respectively, Official Bulletin of the Kingdom of Morocco, Moroccan Official Bulletin: Rabat, Morocco, 5062, 2002, pp. 1518–1525.
[37] H. Dach, Comparison of Nanofiltration and Reverse Osmosis Processes for a Selective Desalination of Brackish Water Feeds, Engineering Sciences [Physics]. Université d'Angers, 2008. Available at: https://tel.archivesouvertes.fr/tel-00433513
[38] S. El-Ghzizel, H. Zeggar, M. Tahaikt, F. Tiyal, A. Elmidaoui, M. Taky, Nanofiltration process combined with electrochemical disinfection for drinking water production: feasibility study and optimization, J. Water Process Eng., 36 (2020) 101225, doi: 10.1016/j.jwpe.2020.101225.
[39] J. Guo, H. Bao, Y. Zhang, X. Shen, J.-K. Kim, J. Ma, L. Shao, Unravelling intercalation-regulated nanoconfinement for durably ultrafast sieving graphene oxide membranes, J. Membr. Sci., 619 (2021) 118791, doi: 10.1016/j.memsci.2020.118791.
[40] S.I. Bouhadjar, H. Kopp, P. Britsch, S.A. Deowan, J. Hoinkis, J. Bundschuh, Solar powered nanofiltration for drinking water production from fluoride-containing groundwater – a pilot study towards developing a sustainable and low-cost treatment plant, J. Environ. Manage., 231 (2019) 1263–1269.
[41] L. Nghiem, A. Schaefer, M. Elimelech, Nanofiltration of hormone mimicking trace organic contaminants, Sep. Sci. Technol., 40 (2005) 2633–2649.
[42] J.F. Fernández, B. Jastorff, R. Störmann, S. Stolte, J. Thöming, thinking in terms of structure–activity-relationships (T-SAR): a tool to better understand nanofiltration membranes, Membranes, 1 (2011) 162–183.
[43] O.T. Mahlangu, B.B. Mamba, Interdependence of contributing factors governing dead-end fouling of nanofiltration membranes, Membranes (Basel), 11 (2021) 47, doi: 10.3390/membranes11010047.
[44] Q. Li, M. Elimelech, Natural organic matter fouling and chemical cleaning of nanofiltration membranes, Water Sci. Technol. Water Supply, 4 (2004) 245–251.
[45] H. Kelewou, A. Lhassani, M. Merzouki, P. Drogui, B. Sellamuthu, Salts retention by nanofiltration membranes: physicochemical and hydrodynamic approaches and modeling, Desalination, 277 (2011) 106–112.
[46] L. Paugam, S. Taha, G. Dorange, P. Jaouen, F. Quéméneur, Mechanism of nitrate ions transfer in nanofiltration depending on pressure, pH, concentration and medium composition March, J. Membr. Sci., 231 (2004) 37–46.
[47] J. Touir, S. Kitanou, M. Zait, S. Belhamidi, M. Belfaquir, M. Tahaikt, M. Taky, A. Elmidaoui, The comparison of electrodialysis and nanofiltration in nitrate removal from groundwater, Indonesian J. Sci. Technol., 6 (2021) 17–30.
[48] F.G. Donnan, Theory of membrane equilibria and membrane potential in the presence of non-dialyzing electrolytes. A contribution to physical–chemical physiology, J. Membr. Sci., 100 (1995) 45–55.

[49] M. Tahaikt, S. El-Ghzizel, N. Essafi, M. Hafsi, M. Taky, A. Elmidaoui. Technical-economic comparison of nanofiltration and reverse osmosis in the reduction of fluoride ions from groundwater: experimental, modeling and cost estimate, Desal. Water Treat., 216 (2021) 83–95.
[50] S. Bunani, E. Yorükoglu, G. Sert, Ü. Yüksel, M. Yüksel, N. Kabay, Application of nanofiltration for reuse of municipal wastewater and quality analysis of product water, Desalination, 315 (2013) 33–36.
[52] S. Shanmuganathan, S. Vigneswaran, T.V. Nguyen, P. Loganathan, J. Kandasamy, Use of nanofiltration and reverse osmosis in reclaiming micro-filtered biologically treated sewage effluent for irrigation, Desalination, 364 (2015) 119–125.